ISSN 1674-1056
http://cpb.iphy.ac.cn
http://iopscience.iop.org/cpb
中国物理 B
Chinese Physics
中国物理 Chinese Physics B

Enhanced thermoelectric performance in p-type Mg_3Sb_2 via lithium doping

Hao Wang(王浩), Jin Chen(陈进), Tianqi Lu(陆天奇), Kunjie Zhu(朱坤杰), Shan Li(李珊), Jun Liu(刘军), Huaizhou Zhao(赵怀周)
Citation: Chin. Phys. B . 2018, 27(4): 047212. **doi:** 10.1088/1674-1056/27/4/047212

Journal homepage: http://cpb.iphy.ac.cn; http://iopscience.iop.org/cpb

What follows is a list of articles you may be interested in

Se substitution and micro-nano-scale porosity enhancing thermoelectric Cu_2Te

Xiaoman Shi(史晓曼), Guoyu Wang(王国玉), Ruifeng Wang(王瑞峰), Xiaoyuan Zhou(周小元), Jingtao Xu(徐静涛), Jun Tang(唐军), Ran Ang(昂然)
Chin. Phys. B . 2018, 27(4): 047204. **doi:** 10.1088/1674-1056/27/4/047204

Effect of Nb doping on microstructures and thermoelectric properties of $SrTiO_3$ ceramics

Da-Quan Liu(刘达权), Yu-Wei Zhang(张玉伟), Hui-Jun Kang(康慧君), Jin-Ling Li(李金玲), Xiong Yang(杨雄), Tong-Min Wang(王同敏)
Chin. Phys. B . 2018, 27(4): 047205. **doi:** 10.1088/1674-1056/27/4/047205

Enhanced thermoelectric properties of p-type polycrystalline SnSe by regulating the anisotropic crystal growth and Sn vacancy

Chengyan Liu(刘呈燕), Lei Miao(苗蕾), Xiaoyang Wang(王潇漾), Shaohai Wu(伍少海), Yanyan Zheng(郑岩岩), Ziyang Deng(邓梓阳), Yulian Chen(陈玉莲), Guiwen Wang(王桂文), Xiaoyuan Zhou(周小元)
Chin. Phys. B . 2018, 27(4): 047211. **doi:** 10.1088/1674-1056/27/4/047211

Multinary diamond-like chalcogenides for promising thermoelectric application

Dan Zhang(张旦), Hong-Chang Bai(白洪昌), Zhi-Liang Li(李志亮), Jiang-Long Wang(王江龙), Guang-Sheng Fu(傅广生), Shu-Fang Wang(王淑芳)
Chin. Phys. B . 2018, 27(4): 047206. **doi:** 10.1088/1674-1056/27/4/047206

Enhanced thermoelectric performance through homogenously dispersed MnTe nanoparticles in p-type $Bi_{0.52}Sb_{1.48}Te_3$ nanocomposites

Tian-Qi Lu(陆天奇), Peng-Fei Nan(南鹏飞), Si-Long Song(宋思龙), Xin-Yue Zhu(朱欣悦), Huai-Zhou Zhao(赵怀周), Yuan Deng(邓元)
Chin. Phys. B . 2018, 27(4): 047207. **doi:** 10.1088/1674-1056/27/4/047207

SPECIAL TOPIC—Recent advances in thermoelectric materials and devices

Enhanced thermoelectric performance in p-type Mg_3Sb_2 via lithium doping*

Hao Wang(王浩)[1,2], Jin Chen(陈进)[1,2], Tianqi Lu(陆天奇)[2], Kunjie Zhu(朱坤杰)[1], Shan Li(李珊)[2], Jun Liu(刘军)[1,†], and Huaizhou Zhao(赵怀周)[2,‡]

[1] School of Materials Science and Engineering, Central South University, Changsha 410083, China

[2] Beijing National Laboratory for Condensed Matter Physics, Institute of Physics, Chinese Academy of Sciences, Beijing 100190, China

(Received 22 January 2018; revised manuscript received 5 March 2018; published online 29 March 2018)

The Zintl compound Mg_3Sb_2 has been recently identified as promising thermoelectric material owing to its high thermoelectric performance and cost-effective, nontoxicity and environment friendly characteristics. However, the intrinsically p-type Mg_3Sb_2 shows low figure of merit ($zT = 0.23$ at 723 K) for its poor electrical conductivity. In this study, a series of $Mg_{3-x}Li_xSb_2$ bulk materials have been prepared by high-energy ball milling and spark plasma sintering (SPS) process. Electrical transport measurements on these materials revealed significant improvement on the power factor with respect to the undoped sample, which can be essentially attributed to the increased carrier concentration, leading to a maximum zT of 0.59 at 723 K with the optimum doping level $x = 0.01$. Additionally, the engineering zT and energy conversion efficiency are calculated to be 0.235 and 4.89%, respectively. To our best knowledge, those are the highest values of all reported p-type Mg_3Sb_2-based compounds with single element doping.

Keywords: p-type Mg_3Sb_2 Zintl compounds, lithium doping, carrier concentration, enhanced thermoelectric properties

PACS: 72.20.Pa, 73.50.Lw **DOI:** 10.1088/1674-1056/27/4/047212

1. Introduction

To recover the massive global-existing waste heat dissipated from industrial or civilian sources to useful energies, thermoelectric (TE) has been one of the most desirable solutions owing to their capability to convert energy between heat and electricity reversibly and directly.[1–4] The performance of TE materials is primarily governed by its dimensionless figure of merit (zT), which is defined as follows: $zT = (S^2\sigma/K)T$, where S represents the Seebeck coefficient, σ is the electrical conductivity, K is the thermal conductivity, and T is the absolute temperature.[5–10] Thus, a good TE material should not only possess high power factor ($PF = S^2\sigma$) but also low thermal conductivity. However, because of the interrelated relationship between electrical and thermal transports through heat-carrying charge carriers, it's extremely difficult to decouple these transports and achieve desirable enhancements on zT property.

The "phonon–glass, electron–crystal" (PGEC) concept introduced by Slack[11] has been an effective way to partially decouple those electrical and thermal parameters for optimizing thermoelectric properties. According to this concept, ideal TE materials prone to have independent functional modules to modulate electron and phonon transport separately. Through optimization on these modules, materials with electron transport characteristics of crystal and phonon transport characteristics similar to glass can be obtained. Among notable families of TE materials such as lead telluride,[12] skutterudites,[13] half-heuslers,[6] MgAgSb,[14] and so on, Zintl phase compounds are found to meet such criterions. It consists of anions (post-transition elements from group 13–15) and cations (alkali metal or alkaline earth metal elements) which exhibits large electronegativity difference.[15,16] During the formation of ionic bonds, the cations donate electrons to the anions while the latter would further build covalent bonds among themselves to satisfy valence balance, thus leading to formation of complicated lattice structure. The stable covalent-bond lattice contributes to the characteristic of "electron crystal", which would dominate the electrical conductivity of the material. In addition, anions in the weak ionic bonding area would form locally disordered structure, offering it the characteristics of the "phonon glass".

Over the past decade, significant progresses have been made on Zintl phase thermoelectric materials, a large number of high performance Zintl phase bulk materials such as $Yb_{14}MnSb_{11}$,[17] $BaGa_2Sb_2$,[18] $Ca_xYb_{1-x}Zn_2Sb_2$,[19] $Ba_{24}In_xGe_{100-x}$,[20] and $NaGaSn_2$[21] have been reported. However, they are restricted in the practical applications for

*Project supported by the National Natural Science Foundation of China (Grant Nos. U1601213 and 51572287) and the Key Research Program of Frontier Sciences of the Chinese Academy of Sciences (Grant No. QYZDB-SSW-SLH013).

†Corresponding author. E-mail: liujun4982004@csu.edu.cn

‡Corresponding author. E-mail: Hzhao@iphy.ac.cn

© 2018 Chinese Physical Society and IOP Publishing Ltd

their toxic or expensive constituent elements. Recently, a cheap and nontoxic Zintl phase compound, Mg_3Sb_2, has greatly attracted the attentions. The Bi and Te co-doped n-type Mg_3Sb_2 bulk material was prepared with good reproducibility using ball milling and SPS method, in which zT value achieved 1.5 at 723 K.[22] Thus indicates the Mg_3Sb_2-based bulk material might be promising thermoelectric materials with potential application in the middle temperature ranges.[23–27] However, the practical application is severely limited by the poor thermoelectric performance of p-type Mg_3Sb_2 materials, which is the direct motivation of this study.

For undoped Mg_3Sb_2, it shows a persistent p-type characteristic since the thermally activated vacancies at Mg-sites with negative charges. However, its low carrier concentration results in a poor electrical conductivity. A variety of approaches have been used to solve this problem, such as doping Pb,[28] Bi[29] at the Sb site, or doping Na,[30] Ag,[31] Mn,[32] Zn[33] at the site of Mg. Among them, Na doping seems to be the most effective way to increase the carrier concentration, but this also increased the lattice thermal conductivity of the material. Other dopants could reduce the thermal conductivity, while the improvement on electrical transport is less satisfactory.

In this work, the alkali metal lithium is used to dope at cationic site in Mg_3Sb_2 to tune the carrier concentration. Experimental results reveal that the doping operation effectively improved the electrical transport performance of the Li-doped samples. Meanwhile, a slightly decrease of the lattice thermal conductivity is observed, which should be attributed to the increased point defects scattering on phonon. As a result, improved TE properties have been achieved in a broad range of temperatures. The peak zT of $Mg_{2.99}Li_{0.01}Sb_2$ bulk material reached 0.59 at 723 K, increased by 158% compared with the un-doped sample. Moreover, the calculated engineering zT and efficiency are 0.235 and 4.89%, respectively, indicating that Li-doped Mg_3Sb_2 compound could be a good p-type thermoelectric material.

2. Experimental methods

2.1. Synthesis

The $Mg_{3-x}Li_xSb_2$ ($x = 0$, 0.005, 0.01, 0.02) bulk samples were prepared by ball milling and spark plasma sintering (SPS). In a typical method, magnesium (Mg, Alfa Aesar, 99.8%, turnings), lithium (Li, Sigma Aldrich, 99.9%, ribbon), and antimony (Sb, Alfa Aesar, 99.999%, pieces) were weighed according to the stoichiometry in an Ar-filled glove box. Then the raw materials were loaded into a stainless steel jar and ball milled for 10 h by using a SPEX Sample Prep 8000 Mixer/Mill. Finally, the obtained powder was put into a graphite die (diameter, 12.7 mm) and treated by SPS process at 1023 K for 10 min under a pressure of 50 MPa. The density of those as-pressed samples was measured by using Archimedes method to be in the range of 96% to 98% of the theoretical density.

2.2. Phase and microstructure analysis

The x-ray diffraction (XRD) patterns of as-prepared samples were collected by a diffractometer (PANalytical X'Pert Pro) operated at 40 kV and 40 mA with Cu Kα radiation ($\lambda = 1.542$ Å). The measurement was carried out in the 2θ range of 20°–80° in air. The microstructures of samples were characterized by a scanning electron microscopy (SEM, XL30S-FFG) on the samples' cross sections. More details were obtained on a transmission electron microscopy (TEM, JEM-2100 Plus).

2.3. Thermoelectric transport measurement

The temperature dependence of electrical resistivity and Seebeck coefficient were measured on a commercial system (LSR-3, Linseis) in the atmosphere of high purity helium. The temperature dependence of total thermal conductivity was defined as $K_{tot} = DC_pd$. Where D represents the thermal diffusivity, C_p is the specific heat capacity calculated by the Dulong–Petit law $C_p = 3NR$, where R is the gas constant, N is the ratio of atomic number to molar mass, d is the density which is measured by Archimedes method. The thermal diffusivities of all samples were measured by the laser flash method using a commercial system (LFA-1000, Linseis). The room-temperature carrier concentration and mobility of all samples were collected by using the van der Pauw method under a magnetic field of 0.5 T.

3. Results and discussion

3.1. Structures and morphologies analysis

As shown in Fig. 1(a), the XRD patterns of as prepared $Mg_{3-x}Li_xSb_2$ compounds can be indexed to the pure Mg_3Sb_2 phase with a space group of $P\bar{3}m1$ (NO. 164). Besides, no obvious peak position shift is observed, which indicates the changes of lattice parameters by lithium doping are negligible. To identify this, the lattice parameters of the doped $Mg_{3-x}Li_xSb_2$, as a function of the various lithium contents, are displayed in Fig. 1(b). The minor change between the doped and undoped samples is attributed to the very small content of dopants, which is consistent with previous reports.[30,31]

Figure 2 shows the typical microstructure of the optimal $Mg_{2.99}Li_{0.01}Sb_2$ sample. The SEM image is displayed in Fig. 2(a), it can be seen that the prepared bulk sample is dense without obvious preferred orientation, and the grain sizes are in the tens of macrons. Figure 2(b) shows the highresolution transmission electron microscopy (HRTEM) image for the same sample, revealing the randomly orientated grains with the interplanar distance of the planes (011) (0.351 nm), (012)

(0.266 nm), and (110) (0.23 nm) of Mg_3Sb_2 phase (JCPDS 36-1180). The nano domains of crystallites in the grain should be favorable for the heating-carrying phonon scattering in this material, as discussed in the following content.

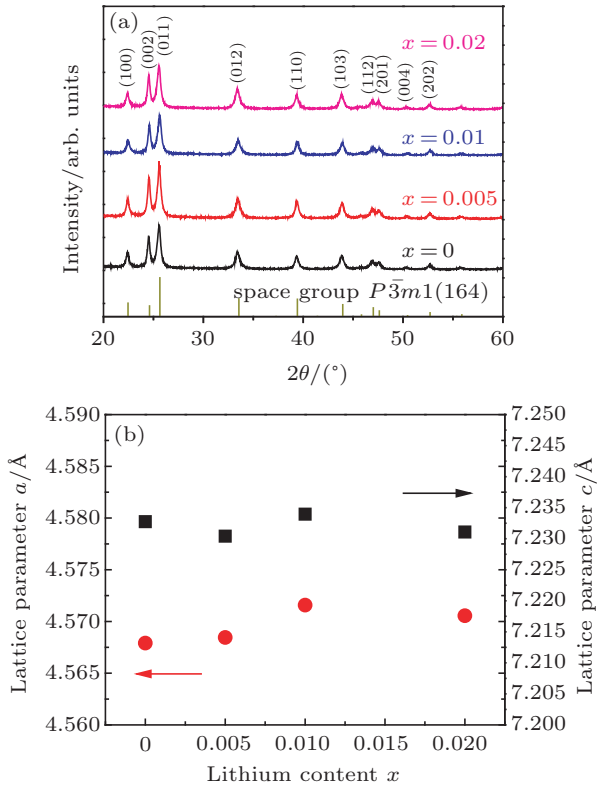


Fig. 1. (color online) (a) XRD patterns and (b) lithium doping dependence of lattice parameters for series of Li-doped $Mg_{3-x}Li_xSb_2$ ($x = 0$, 0.005, 0.01, 0.02) compounds.

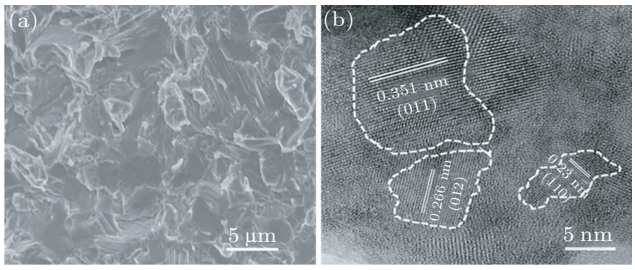


Fig. 2. (a) SEM and (b) high resolution TEM image of as-synthesized $Mg_{2.99}Li_{0.01}Sb_2$ sample.

3.2. Electrical transport analysis

The temperature dependence of electrical resistivity and Seebeck coefficient are shown in Fig. 3. Among them, figure 3(a) reveals that the electrical resistivity of the Li-doped materials has been reduced drastically even though small amounts of lithium were doped in. To explain this phenomenon, the results of room-temperature Hall measurements are displayed as shown in Fig. 4(a). Carrier concentration (n) of undoped sample is 0.227×10^{19} cm^{-3}, while it can be increased to 3.211×10^{19} cm^{-3} (about 14 times higher than the former) when doped only 0.2 at.% ($x = 0.005$) Li at Mg site. Nevertheless, the carrier mobility (μ) of this doped sample decreases only by 12.5% compared to the undoped one. For

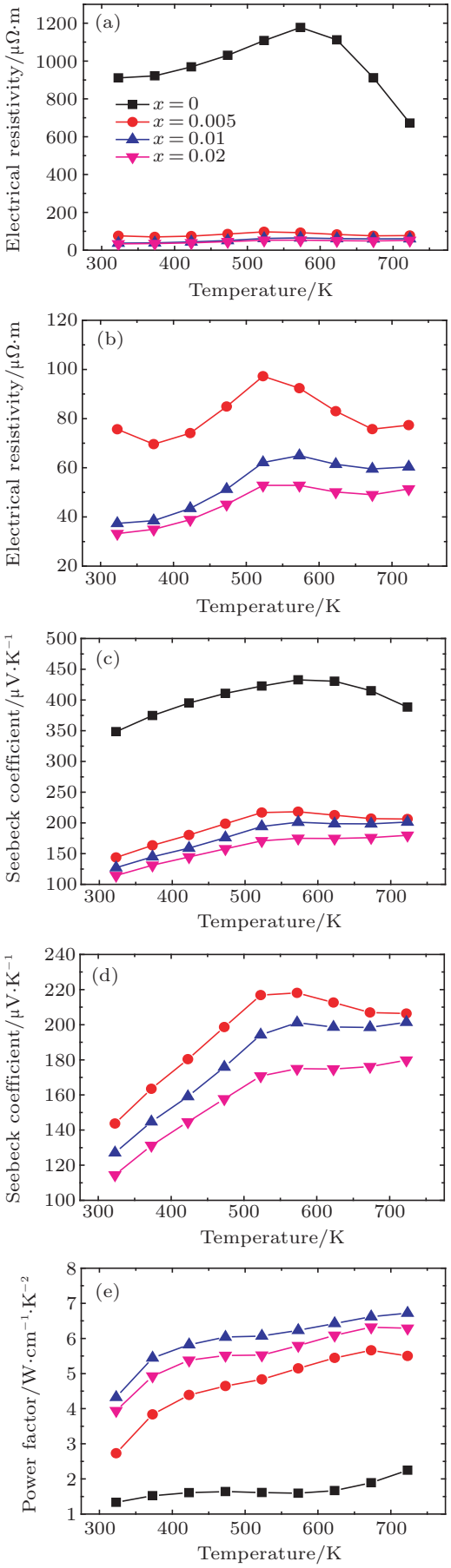


Fig. 3. (color online) Temperature dependence of (a) electrical resistivity and (c) Seebeck coefficient for all prepared samples; (b) electrical resistivity and (d) Seebeck coefficient for Li-doped samples.

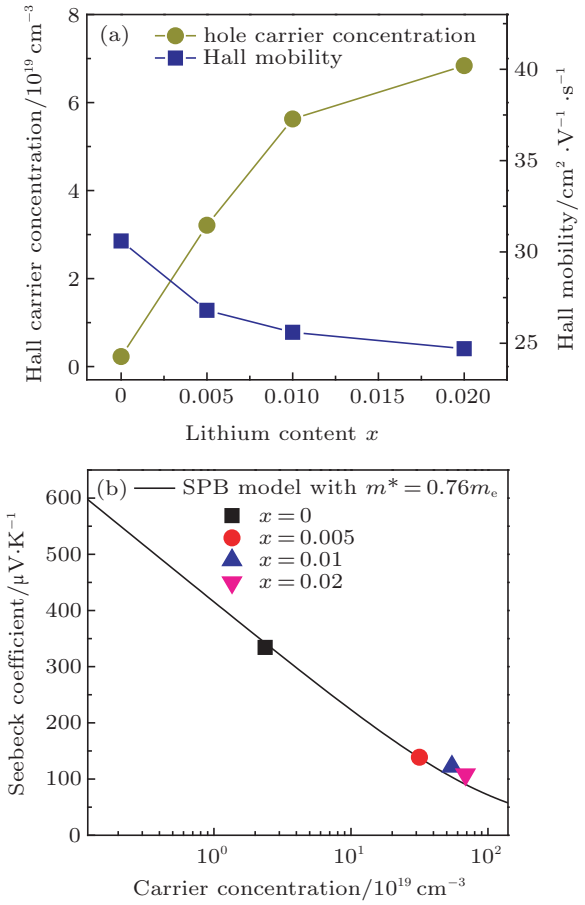


Fig. 4. (color online) (a) Room-temperature Hall carrier concentration and Hall mobility of $Mg_{3-x}Li_xSb_2$ ($x = 0$, 0.005, 0.01, 0.02), (b) the Seebeck coefficient versus carrier concentration at room temperature. The black solid curve is the calculated relation between Seebeck coefficient and carrier concentration using an SPB model with $m^* = 0.76m_e$, while the scatters represent the experimental data of $Mg_{3-x}Li_xSb_2$ ($x = 0$, 0.005, 0.01, 0.02) compounds.

electrical conductivity $\sigma = ne\mu$, the improved electronic property of doped samples can be ascribed to their higher carrier concentration. More details can be found from Fig. 3(b) which shows the electrical resistivity of these doped materials. As can be seen, the electrical resistivity decreases in the whole temperature range with increasing Li content. In addition, the temperature dependence of electrical resistivity for all samples can be separated into two regimes. From 323 K to 573 K, it is characterized by heavily degenerated semiconductor, then change into semiconductor features during 573 K–723 K owing to the intrinsic thermal excitation at high temperature. Figure 3(c) and 3(d) show the Seebeck coefficient as a function of temperature for all samples. The positive value suggests that they are p-type semiconductors which are consistent with the results of Hall measurement. It also exhibits the similar temperature dependent characteristic as the electrical resistivity discussed above. Figure 3(e) is the temperature-dependent power factor of all samples. Apparently, the power factor can be effectively enhanced through a lithium doping process. Besides, for the optimized composition $Mg_{2.99}Li_{0.01}Sb_2$, its power factor reaches 6.72 $\mu W \cdot cm^{-1} \cdot K^{-2}$ at 723 K, which is a relatively high value among all p-type Mg_3Sb_2 materials.

In the approximation of energy independent scattering, the Seebeck coefficient can be described using a single parabolic band (SPB) model:

$$S = \frac{8\pi^2 k_B^2}{3eh^2} m^* T \left(\frac{\pi}{3n}\right)^{2/3}, \tag{1}$$

where k_B is Boltzmann's constant, h is Planck's constant, m^* is the effective mass, n is the carrier concentration, and e is the charge of an electron.[34] The Pisarenko relation at room temperature can be plotted given that the effective mass $m^* = 0.76m_e$ (m_e represents the mass of an electron) as previous work mentioned.[33] As figure 4(b) shows, the experimental room-temperature carrier concentration and Seebeck coefficient of $Mg_{3-x}Li_xSb_2$ ($x = 0$, 0.005) compounds are fitted well with the calculated Pisarenko curve, while a little deviation appears for samples with $x = 0.01$ and 0.02 which caused by the increased effective mass leading by higher doping ratio. Since the change is small, SPB model is still appropriate to describe the electronic transport of those samples.

3.3. Thermal transport analysis

Figure 5(a) shows the temperature dependence of total thermal conductivity (K_{tot}) for the studied samples, it decreases with the increase of temperature. Additionally, it is proportional to the doped Li ratio. Generally, K_{tot} in a TE material is mainly composed of three parts: lattice thermal conductivity (K_l), carrier thermal conductivity (K_e), and bipolar thermal conductivity (K_b). In order to understand the thermal transport mechanism more clearly, the carrier thermal conductivity K_e is given by the Wiedemann–Franz law $K_e = L\sigma T$. L is the Lorenz number which can be calculated by employing the SPB model as follows:[35]

$$L = \left(\frac{k_B}{e}\right)^2 [(1+\lambda)(3+\lambda)F_\lambda(\chi)F_{\lambda+2}(\chi) - (2+\lambda)^2 F_{\lambda+1}(\chi)^2]/[(1+\lambda)^2 F_\lambda(\chi)^2], \tag{2}$$

$$S = \frac{k_B}{e}\left(\frac{(2+\lambda)^2 F_{\lambda+1}(\chi)}{(1+\lambda)F_\lambda(\chi)} - \chi\right), \tag{3}$$

$$F_j(\chi) = \int_0^\infty \frac{\varepsilon^j d\varepsilon}{1+\exp(\varepsilon-\chi)}, \tag{4}$$

where $F_j(\chi)$ represents the Fermi integral, χ is the reduced Fermi level, and ε is the reduced carrier energy. The value of scattering factor λ is set as zero by assuming that the carrier relaxation time is limited by acoustic phonon scattering.[36] Consequently, the Lorenz number L and Seebeck coefficient S are connected through the Fermi integral. However, searching the Fermi integral seems to be a complicated operation. Kim *et al.* simplified the above process to an expression:[37]

$$L = 1.5 + \exp\left[-\frac{|S|}{116}\right], \tag{5}$$

where the unit of L and S are 10^{-8} W·Ω·K^{-2} and μV·K^{-1}, respectively. The accuracy is over 95% for single parabolic band model where acoustic phonon scattering is the dominant scattering mechanism. Considering the typical error range of total thermal conductivity is about 10%, the result of above calculation is credible.

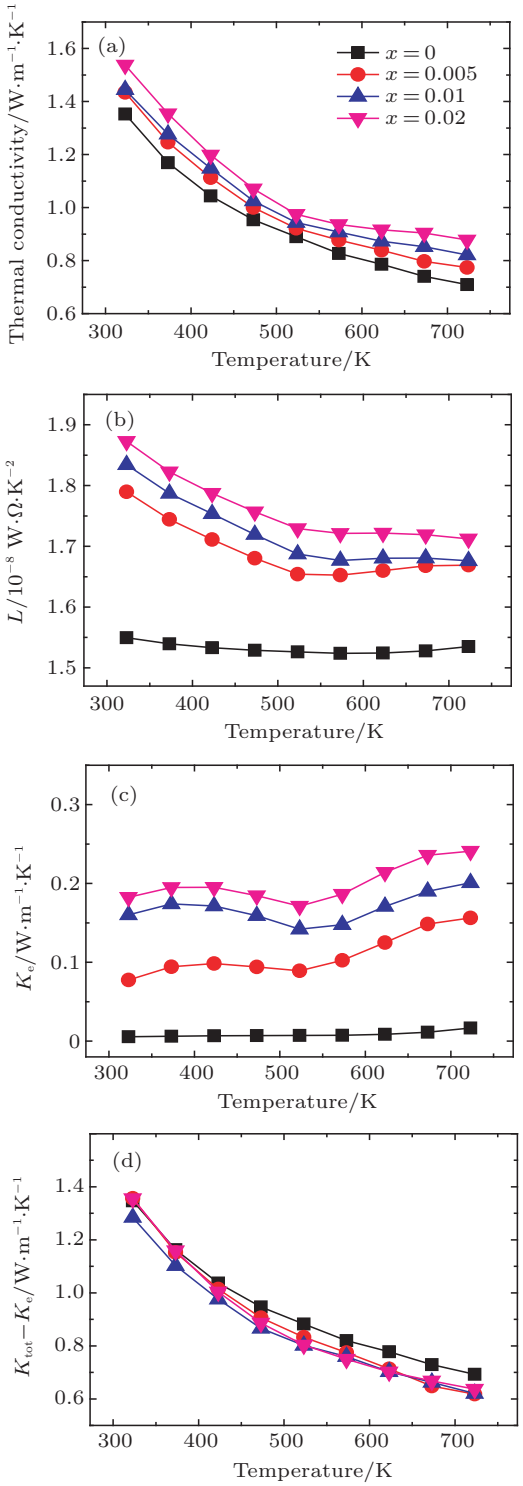


Fig. 5. (color online) Temperature dependence of (a) total thermal conductivity; (b) Lorenz number; (c) carrier thermal conductivity; and (d) lattice thermal conductivity for $Mg_{3-x}Li_xSb_2$ ($x = 0$, 0.005, 0.01, 0.02) samples.

The obtained L and carrier thermal conductivity K_e are shown in Figs. 5(b) and 5(c), respectively. The bipolar thermal conductivity K_b originates from the excitation of minority carriers at a finite temperature and plays a more and more important role with the increase of temperature. In this study, the bipolar effect is not obvious because there is little reduction of Seebeck coefficient caused by it in high temperature. So, as plotted in Fig. 5(d), the lattice thermal conductivity can be estimated roughly by subtracting K_e from the total thermal conductivity K_{tot}, showing a T^{-1}-type behavior which means it is dominated by the Umklapp process. Among the four plots in Fig. 5, the carrier thermal conductivity of doped samples increases substantially with increasing Li content, while the lattice thermal conductivity of them are lower than that of the undoped sample. This is mainly ascribed to the increased point defects scattering produced by Li dopants. Therefore, the increased total thermal conductivity of Li-doped samples is contributed by the higher carrier thermal conductivity resulted from their enhanced electrical properties. Compared with the Na-doped materials (in which lattice thermal conductivity increased anomalously with increasing Na content),[30] the smaller value of total thermal conductivity for Li-doped samples is reasonable owing to its lower lattice thermal conductivity.

3.4. Calculation of *zT* and efficiency

The calculated Figure of merit (zT) is shown in Fig. 6(a). Owing to the optimized electrical transport performance, the peak zT of optimal $Mg_{2.99}Li_{0.01}Sb_2$ bulk material reaches 0.59 at 723 K, about 2.58 times higher than that of the un-doped sample. Furthermore, in terms of the global TE performance over a wide temperature range, the engineering zT ((zT_{eng}) proposed by Kim *et al.*[38] can be used to reflect the practical efficiency of a TE material since the TE devices always works under a temperature gradient, which is defined as:

$$(zT)_{eng} = \frac{\left(\int_{T_c}^{T_h} S(T)\,dT\right)^2}{\int_{T_c}^{T_h} \rho(T)\,dT \int_{T_c}^{T_h} k(T)\,dT}\Delta T, \tag{6}$$

where $\Delta T = T_h - T_c$, T_h is the hot-side temperature, T_c is the cold side temperature. $S(T)$, $\rho(T)$, and $k(T)$ are measured temperature-dependent Seebeck coefficient, electrical resistivity, and total thermal conductivity, respectively. Figure 6(b) shows the ΔT dependence of engineering zT with $T_c = 323$ K for all samples. It can be clearly seen that the $(zT)_{eng}$ values of the doped samples are substantially enhanced compared with that of the pristine sample, especially for the $Mg_{2.99}Li_{0.01}Sb_2$ compound which $(zT)_{eng}$ arrives 0.235 when $\Delta T = 400$ K. Moreover, the related energy conversion efficiency (η) is expressed as:

$$\eta = \eta_c \frac{\sqrt{1+(zT)_{eng}(\hat{a}/\eta_c - 1/2)} - 1}{\hat{a}\left(\sqrt{1+(zT)_{eng}(\hat{a}/\eta_c - 1/2)} + 1\right) - \eta_c}, \tag{7}$$

$$\eta_c = \frac{T_h - T_c}{T_h}, \tag{8}$$

$$\hat{a} = \frac{S(T_h)\Delta T}{\int_{T_c}^{T_h} S(T)\mathrm{d}T}, \tag{9}$$

where η_c represents Carnot efficiency, $\hat{a}$ is a dimensionless intensity factor of the Thompson effect, $S(T_h)$ is the Seebeck coefficient at the hot-side. Thus, there is a positive correlation between η and $(zT)_{eng}$. From Fig. 6(c), the efficiency of $Mg_{2.99}Li_{0.01}Sb_2$ approaches 4.89% at $\Delta T = 400$ K, about 190% higher than that of the undoped sample.

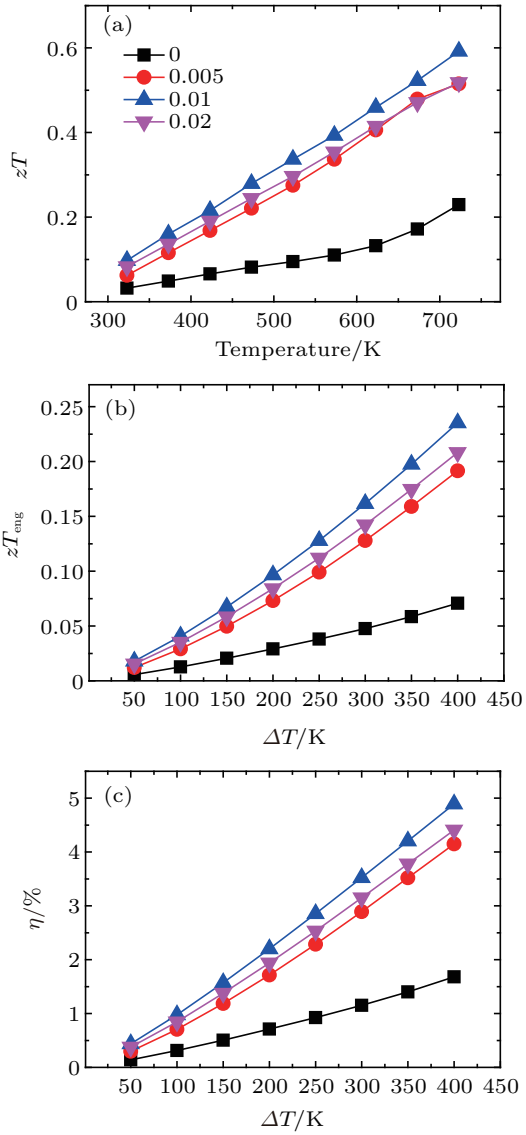


Fig. 6. (color online) Calculated thermoelectric performance of $Mg_{3-x}Li_xSb_2$ ($x = 0$, 0.005, 0.01, 0.02) compounds: (a) zT; (b) engineering zT; and (c) energy conversion efficiency.

To further evaluate the impact of different dopants (such as Li, Na, Ag, Pb, Bi) on the TE performance of Mg_3Sb_2, figure 7 shows the zT and $(zT)_{eng}$ of those doped samples. It is observed that the zT (shown in Fig. 7(a)) of Li-doped sample increases linearly with temperature and exhibits the highest value in a broad of test temperature range (except for the Pb-doped sample over 630 K and Ag-doped sample below 400 K). Besides, the Li-doped compound also exhibits the highest $(zT)_{eng}$ (when $T_h = 723$ K, $T_c = 323$ K) among them, as shown in Fig. 7(b). Therefore, it is reasonable to conclude that Li is a more effective acceptor dopant.

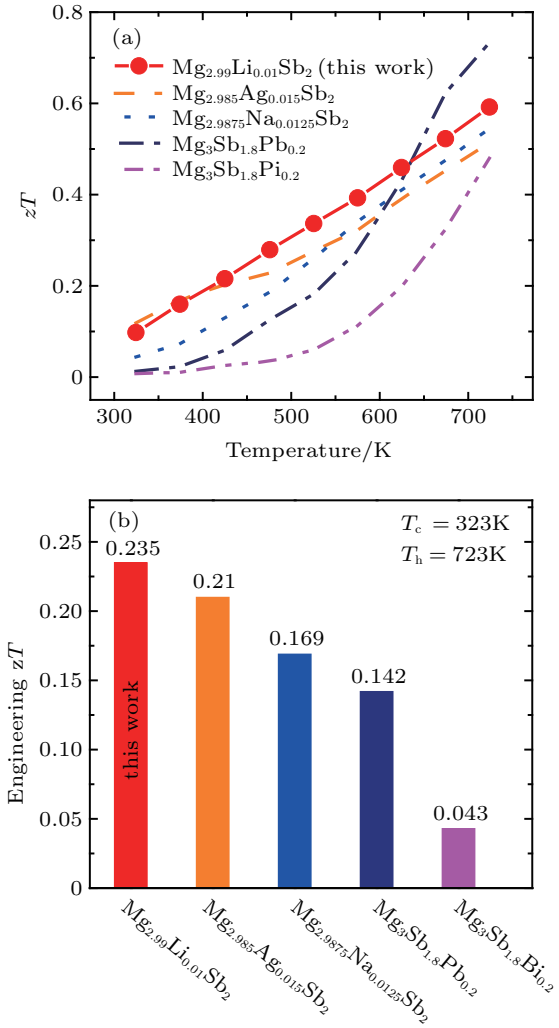


Fig. 7. (color online) Comparison of (a) temperature-dependent zT and (b) engineering zT of $Mg_{2.99}Li_{0.01}Sb_2$ and those of previous reported p-type Mg_3Sb_2 compounds ($Mg_{2.985}Ag_{0.015}Sb_2$, $Mg_{2.9875}Na_{0.0125}Sb_2$, $Mg_3Sb_{1.8}Pb_{0.2}$, and $Mg_3Sb_{1.8}Bi_{0.2}$).

4. Conclusions

In summary, a series of Li-doped p-type $Mg_{3-x}Li_xSb_2$ ($x = 0$, 0.005, 0.01, 0.02) bulk material has been prepared by combination of ball milling and SPS process. The thermoelectric performance was greatly improved in comparison to that of undoped Mg_3Sb_2 sample. For the optimized $Mg_{2.99}Li_{0.01}Sb_2$ sample, the peak zT and maximum $(zT)_{eng}$ reaches to 0.59 and 0.235, respectively. This enhancement can be mainly ascribed to the improved electrical transport properties by optimizing carrier concentration via effective Li doping at Mg site. In addition, Li-doped sample shows the best global TE performance among other single-element-doped Mg_3Sb_2 materials, thus pushing the practical application of Mg_3Sb_2 based Zintl compounds one step further.

References

[1] Bell L E 2008 *Science* **321** 1457
[2] Disalvo F J 1999 *Science* **285** 703
[3] Harman T C, Taylor P J, Walsh M P and LaForge B E 2002 *Science* **297** 2229
[4] Kraemer D, Poudel B, Feng H-P, Caylor J C, Yu B, Yan X, Ma Y, Wang X, Wang D, Muto A, McEnaney K, Chiesa M, Ren Z and Chen G 2011 *Nat. Mater.* **10** 532
[5] Pei Y, Shi X, LaLonde A, Wang H, Chen L and Snyder G J 2011 *Nature* **473** 66
[6] Zhao H Z, Cao B L, Li S M, Liu N, Shen J W, Li S, Jian J K, Gu L, Pei Y h, Snyder G J, Ren Z F and Chen X L 2017 *Adv. Energy Mater.* **7** 1700446
[7] Zhao L D, Tan G, Hao S, He J, Pei Y, Chi H, Wang H, Gong S, Xu H and Dravid V P 2016 *Science* **351** 141
[8] Wu Z H, Xie H Q, Wang Y Y, Xing J J and Mao J H 2015 *Chin. Phys. Lett.* **32** 131
[9] Xu Y 2016 *Chin. Phys. B* **25** 54
[10] Zhang X, Liu J, Li Y, Su W B, Li J C, Zhu Y H, Li M K, Wang C M and Wang C L 2015 *Chin. Phys. Lett.* **32** 113
[11] Slack G A 1995 *CRC Handbook of Thermoelectrics* (Boca Raton: CRC Press) p. 407
[12] Ruan L, Luo J, Zhu H, Zhao H and Liang J 2015 *J. Electron. Mater.* **44** 3556
[13] Shi X, Kong H, Li C P and Uher C 2008 *Appl. Phys. Lett.* **92** 407
[14] Li D D, Zhao H Z, Li S M, Wei B P, Shuai J, Shi C L, Xi X K, Sun P J, Meng S, Gu L, Ren Z F and Chen X L 2015 *Adv. Func. Mater.* **25** 6478
[15] Kauzlarich S M,Brown S R and Jeffrey Snyder G 2007 *Dalton Transactions* **21** 2099
[16] Toberer E S, May A F and Snyder G J 2010 *Chem. Mater.* **22** 624
[17] Brown S R, Kauzlarich S M, Gascoin F and Snyder G J 2006 *Chem. Mater.* **18** 1873
[18] Kim S J and Kanatzidis M G 2001 *Inorg. Chem.* **40** 3781
[19] Gascoin F, Ottensmann S, Stark D, Haïe S M and Snyder G J 2005 *Adv. Func. Mater.* **15** 1860
[20] Kim J H, Okamoto N L, Kishida K, Tanaka K and Inui H 2007 *J. Appl. Phys.* **102** 094506
[21] Yamada T, Yamane H and Nagai H 2015 *Adv. Mater.* **27** 4708
[22] Tamaki H, Sato H K and Kanno T 2016 *Adv. Mater.* **28** 10182
[23] Jing S, Mao J, Song S, Zhu Q, Sun J, Wang Y, He R, Zhou J, Singh D J and Chen G 2017 *Energy Environ. Sci.* **10** 799
[24] Mao J, Shuai J, Song S, Wu Y, Dally R, Zhou J, Liu Z, Sun J, Zhang Q and Dela C C 2017 *Proc. Natl. Acad. Sci. USA* **114** 10548
[25] Mao J, Wu Y, Song S, Shuai J, Liu Z, Pei Y and Ren Z 2017 *Mater. Today Phys.* **3** 1
[26] Mao J, Wu Y, Song S, Zhu Q, Shuai J, Liu Z, Pei Y and Ren Z 2017 *Acs Energy Lett.* **2** 2245
[27] Zhang J, Song L, Pedersen S H, Yin H, Hung L T and Iversen B B 2017 *Nat. Commun.* **8** 13901
[28] Bhardwaj A and Misra D K 2014 *RSC Adv.* **4** 34552
[29] Bhardwaj A, Rajput A, Shukla A K, Pulikkotil J J, Srivastava A K, Dhar A, Gupta G, Auluck S, Misra D K and Budhani R C 2013 *RSC Adv.* **3** 8504
[30] Shuai J, Wang Y, Kim H S, Liu Z, Sun J, Chen S, Sui J and Ren Z 2015 *Acta Mater.* **93** 187
[31] Song L, Zhang J and Iversen B B 2017 *J. Mater. Chem. A* **5** 4932
[32] Kim S, Kim C, Hong Y K, Onimaru T, Suekuni K, Takabatake T and Jung M H 2014 *J. Mater. Chem.* **2** 12311
[33] Bhardwaj A, Chauhan N S, Goel S, Singh V, Pulikkotil J J, Senguttuvan T D and Misra D K 2016 *Phys. Chem. Chem. Phys.* **18** 6191
[34] Cutler M, Leavy J F and Fitzpatrick R L 1964 *Phys. Rev.* **133** A1143
[35] May A F, Toberer E S, Saramat A and Snyder G J 2009 *Phys. Rev. B* **80** 125205
[36] Wood C 1988 *Rep. Prog. Phys.* **51** 459
[37] Kim H S, Gibbs Z M, Tang Y, Wang H and Snyder G J 2015 *APL Mater.* **3** 041506
[38] Kim H, Liu W, Chen G, Chu C and Ren Z 2015 *Proc. Natl. Acad. Sci. USA* **112** 8205